Instabilities triggered in different conducting fluid geometries due to slowly time-dependent magnetic fields

I. Cortés-Domínguez, and J. Burguete

Citation: Chaos **28**, 075514 (2018); doi: 10.1063/1.5027674
View online: https://doi.org/10.1063/1.5027674
View Table of Contents: http://aip.scitation.org/toc/cha/28/7
Published by the American Institute of Physics

Instabilities triggered in different conducting fluid geometries due to slowly time-dependent magnetic fields

I. Cortés-Domínguez[a] and J. Burguete[b]
Physics and Applied Mathematics Department, School of Science, University of Navarra, Irunlarrea 1, E-31008 Pamplona, Spain

(Received 5 March 2018; accepted 16 May 2018; published online 23 July 2018)

The main objective of this work is the study and analysis of non-linearities forced through oscillating magnetic fields in a conducting fluid where the instabilities are triggered due to magnetohydrodynamic forces. Different geometries have been studied and different surface patterns that break the symmetries have been observed. First, an InGaSn drop of fluid where the system breaks the azimuthal and radial symmetries depending on the volume is observed. Second, we extend the study to an InGaSn annular configuration where the presence of patterns opens the door to discuss the possibility to extend these results to other configurations as biological systems, where the conducting fluid is an electrolyte. This configuration has an added interest, as it has been proposed that the vertigoes triggered on patients in an MRI test could be generated by the interaction of the magnetic field with the electrolyte present in the inner ear. *Published by AIP Publishing.* https://doi.org/10.1063/1.5027674

In this work, we present experiments where different non-linear dynamics have been obtained on a conducting fluid. The destabilizing mechanism has its origin on a time-dependent magnetic field. This field produces a beating of the fluid generating different patterns. We compare the effect of various geometries (disc-shaped and toroid drops) and relate this problem with a recent description of adverse symptoms (vertigoes and dizziness) on MRI devices.

I. INTRODUCTION

The existence of non-linearities in fluid dynamics is a challenge for the scientific community because it is the source of the complex behavior that appears in many physical processes. These processes cover different scales from extended natural systems (e.g., atmospheric phenomena, ocean flows, stellar flows) to many other applied systems (e.g., aerodynamics, navigation, medicine, microfluidics). There are many factors that affect the fluid dynamics, two of them being the geometry and the boundary conditions. These boundaries can be very different, from solid physical walls to interfaces where the boundaries are defined by the liquid densities, chemical barriers, or magnetic fields.

The effect of the fluid confinement has been analyzed in many different experiments. One of the first experiments was performed by Faraday in 1831, when he analyzed the instabilities due to mechanical oscillations.[1] In these experiments, the flow was totally confined by walls and different standing waves were found and analyzed theoretically[2] and experimentally.[3] Other instabilities in confined systems with small aspect ratio and external forcing have been studied: For example, magnetohydrodynamics (MHD) forces that produce periodic motions and surface waves have been deeply studied theoretically[4] and experimentally;[5] in a slightly different configuration, the instability called Mercury Beating Heart (MHB);[6] and instabilities in levitating fluid droplets by ultrasounds.[8] In all the previous examples, the geometry affects the solutions and the instability thresholds on the parameter space. In spite of the diversity of the different physical processes, generic behaviors can be found in those experiments with different forcing systems and confinements.[7]

In this work, we are interested in the study of one of these forcing mechanisms, the non-linearities produced by oscillating magnetic fields in conducting fluids. The presence of instabilities in liquid metals forced with a low frequency magnetic field in a strong non-linear regime was described by Galpin *et al.*[9] when they observed different surface modulations in a mercury pool emphasizing the presence of parametric resonances as in Faraday's experiments. The observed surface waves were deeply analyzed later by Galpin, Fautrelle, and Sneyd[4,19] detecting the coexistence of axisymmetric and non-axisymmetric patterns. The critical parameter in this problem is called the interaction parameter N that basically represents the ratio between the electromagnetic forces on the fluid, compared to inertia. These instabilities were observed far from threshold, for large values of the bifurcation parameter $N > 1$.

Some years later, Burguete *et al.*[5] observed a similar behavior for smaller values of the bifurcation parameter N forcing an InGaSn droplet with an oscillating magnetic field with non-zero mean. They characterized the presence of non-axisymmetric patterns close to the threshold. Based on this experimental approach, we have previously characterized the existence of patterns for small values of the bifurcation parameter N in an InGaSn droplet using a zero-mean time oscillating magnetic field.[11]

In these experiments, the vertical time-dependent magnetic field produces an oscillating radial Lorentz force that periodically expands and contracts the fluid drop. An axisymmetric pattern is created that can destabilize for specific

[a]Electronic mail: icortesd@unav.es
[b]Electronic mail: javier@unav.es

regions of the parameter space. In some cases, various patterns can coexist for the same experimental parameters and we could observe cycles and other complex dynamics. In order to clarify the mechanisms involved in the pattern formation, the temporal evolution was split into harmonic and sub-harmonic frequencies of the Lorentz forces. There are two different mechanisms that trigger the instabilities associated with each set of modes: surface waves generated by the beating of the droplet that correspond to harmonics of the forcing mechanism frequency; and oscillations for sub-harmonic frequencies that obey a first order Mathieu-Hill equation, predicted by Galpin *et al.*[9] and Fautrelle *et al.*[10]

In this work, we analyze the instabilities that emerge in different geometries of a conducting fluid drop under the action of a time-dependent magnetic field. We analyze the following configurations: disc-shaped drops (hereafter, referred to as drops) and toroidal shaped drops (hereafter, referred to as ring). For the case of disc geometries, azimuthal and radial wavelengths have been observed depending on the droplet volume and different instability threshold regions and power laws have been characterized. For the case of the ring geometry, azimuthal wavenumbers have been observed and studied.

II. EXPERIMENTAL SETUP

Following the approach introduced in Ref. 11, the experimental setup description is divided into three different parts: the geometry of the vessel that holds the liquid; the external magnetic field that forces the system and triggers the instabilities; and the acquisition system.

A. Geometry

The whole study was done using a cylindrical cavity with an inner diameter of 84 mm made of TEFLON® that has low friction coefficient and wettability [central part of Fig. 1(a)]. The bottom inner surface of the experimental cell was designed as a modular plate that can be replaced using different geometries. This work is centered in two different cases: a disk shape with a small depression milled in the center of the plate [Fig. 1(b)] and a ring shape [Fig. 1(c)].

The interface between the fluid and the container is defined filling the vessel with a large drop of a liquid metal alloy. This alloy is a combination of Indium, Gallium, and Tin (InGaSn; density $\rho_{InGaSn} = 6360\,\mathrm{kg/m^3}$, electrical conductivity $\sigma_{InGaSn} = 3.1 \times 10^6\,\mathrm{S/m}$, interfacial tension $\gamma_{InGaSn} = 0.53\,\mathrm{N/m}$). As a consequence of the surface tension, the liquid metal adopts the shape of a thick droplet or a ring. We use this alloy for two main reasons, it has good electrical conductivity and the InGaSn remains liquid at room temperature.[12,13] In order to prevent the oxidation of the eutectic alloy, a volume of 1% water-HCl dilution has been placed with the InGaSn to fill the vessel. The dimensionless Bond number ($Bo = (\Delta\rho g L^2)/\gamma$) gives an idea of the ratio between gravity and surface tension effects, where $\Delta\rho$ is the density difference between the two phases, g is the acceleration due to gravity, L is the characteristic length scale of the flow, and γ is the interfacial tension. In our case, $Bo \gg 1$ so interfacial forces weakly affect the fluid flow. Finally, a transparent cover completes the experimental cell.

B. External magnetic field

The destabilizing force in this experiment is produced by the interaction of a time-dependent magnetic field with the electrical currents generated by the change of the magnetic flux in the conducting fluid. There are different ways to produce this magnetic field, in our case, we generate a time-dependent magnetic field with zero mean.

The magnetic field has its origin in a sinusoidal time-dependent current that flows through a copper coil (Fig. 1). This current is modulated with a homemade variable frequency drive being the magnetic field generated proportional to $B_e = B_0 \sin(\omega_0 t) = B_0 \sin(2\pi f_0 t)$. This variable frequency drive allows an accurate control of frequency and intensity, so the system allows an accurate phase-space instability study. For the maximum circulating current $I = 60\,\mathrm{A}$, the corresponding magnetic field amplitude is $B_0 = 0.07\,\mathrm{T}$.

The experimental cell is placed just in the center of the coil. The magnetic field has been characterized using different Hall probes. The vertical component is nearly constant with variations below 2%. The radial component is null at the center and in any other location remains below 3% of the maximum value of the magnetic field magnitude. From these results, we can assume the magnetic field to be spatially homogeneous.

The power supply that controls the system reaches intensities up to $60\,\mathrm{A} \sim 70\,\mathrm{mT}$. The corresponding frequencies are in the very low frequencies regime with frequencies ranging 0.4-10 Hz. Because of the maximum height of the drops of fluid studied, the proposed frequency range is small enough to ensure that the magnetic field fully penetrates into the drop of fluid avoiding what is known as skin effect. In the worst case scenario (largest frequency), the penetration length is $L_p \approx \sqrt{\frac{2}{\sigma_{InGaSn}\,\mu_0\,\omega_0}} \approx 60\,\mathrm{mm}$, whereas the largest thickness of the experimental drops is $h = 22\,\mathrm{mm}$. So, the forces that destabilize the fluid can be considered bulk forces.

C. Optical system

The last part of the experimental setup is the acquisition system that allows us to recover the forced dynamics. The proposed method consists of a shadowgraphy over the free surface of the liquid metal droplet that has a reflecting surface.[14] A white LED is placed close to the focal point of a parabolic mirror so it illuminates the interface with a parallel beam mostly perpendicular to the liquid metal surface (Fig. 1). The light reflected at the interface is collected with the same mirror and redirected to a camera placed close to the focal point.

When the magnetic field is non-zero, the forces present in the liquid metal destabilize the fluid layer deviating the interface from the equilibrium position. Different flows could be created giving rise to surface modulations. The presence of surface deflections affects the reflection of the parallel beam of light. The intensity recovered by the camera increases in depressed regions of the surface because it concentrates

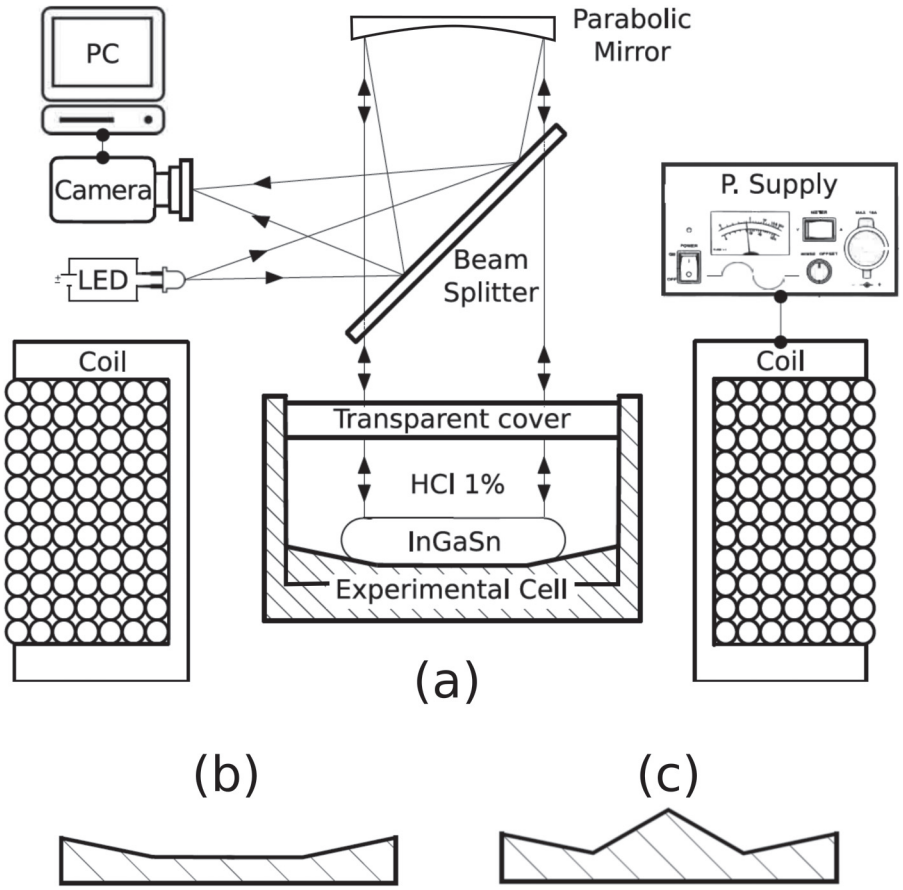

FIG. 1. Experimental setup: (a) Cross section of the container located in the central axis of the coil that produces a sinusoidal magnetic field nearly vertical in the InGaSn volume. The magnetic field is controlled by a home-made variable frequency drive. The optics and acquisition system completes the setup. Modular bottom plates: (b) with a depression milled in the central region: The drop of fluid adopts the form of a thick disc. (c) With a depression along a defined radius: The drop adopts the form of a toroid (ring).

the light (concave regions) when the modulation is small. Conversely, the intensity decreases in convex regions of the surface, while in plane regions the light is reflected without deviation. So, when the instabilities are triggered, the deflection of the surface will be transposed as images with different light intensities. It is possible to study the dynamical behavior of the system as a result of the gray scale between the bright and dark regions that appear due to the modulations. This system allows us to detect surface modulations up to 10 μm and the transverse horizontal resolution is up to 0.3 mm.

III. MHD EFFECTS AND PATTERN FORMATION

A. MHD introduction

The origin of the observed dynamics is the MHD forces.[15] The oscillation of the external magnetic field will induce magnetic flux density modifications across the liquid metal layer. As the InGaSn is a conducting fluid, those variations induce currents in the fluid layer due to Lenz's law that try to balance the varying magnetic flux densities creating an induced magnetic field. These induced currents can be expressed as a current density $\vec{j}$ that interacts with the magnetic field through the Lorentz force.

The equations that govern the behavior of this problem describe the evolution of the velocity field $\vec{u}$ and the global magnetic $\vec{B}$ field. The first one is the Navier Stokes equation, with a new bulk force, the Lorentz force $\vec{F}_L = \vec{j} \times \vec{B}$ that couples the magnetic and velocity fields. The system is closed with the Induction equation that consists of a combination of the Maxwell equations under the MHD approximation[15] and describes the evolution of the total magnetic field $\vec{B}$, i.e., the combination of the external and the induced fields.

The dimensionless forms of these two equations are, for the Navier Stokes equation:

$$\partial_t \vec{u} + [R_m](\vec{u} \cdot \nabla)\vec{u} = -\nabla p + [P_m]\nabla^2 \vec{u} + [N](\nabla \times \vec{B}) \times \vec{B} \tag{1}$$

and the Induction equation:

$$\partial_t \vec{B} = [R_m]\nabla \times (\vec{u} \times \vec{B}) + \nabla^2 \vec{B}, \tag{2}$$

where p stands for the pressure field. The evolution depends on three dimensionless parameters, the interaction parameter N, the magnetic Reynolds number Rm, and the magnetic Prandtl number Pm.

The interaction parameter N represents the ratio between the electromagnetic forces and the inertial forces. This parameter is defined as $N = B_0^2 L\sigma/\rho U$, where B_0 is the amplitude of the forcing magnetic field, L is a characteristic length (typically, the droplet radius), U is a characteristic velocity (assuming the axisymmetry of the geometry, the radial modulation of the fluid surface, $U = fL$, where f is the forcing frequency), and ρ and σ are, respectively, the density and electrical conductivity of the InGaSn alloy. The magnetic Prandtl number $Pm = \nu\mu_0\sigma$, where ν is the kinematic viscosity, expresses the ratio between the viscous forces and the Lorentz forces and depends only on the working fluid. It can be expressed also as the ratio between the magnetic and hydrodynamic Reynolds numbers $Pm = \frac{Rm}{Re}$. Finally, the magnetic Reynolds number $Rm = UL\mu_0\sigma$ represents the ratio

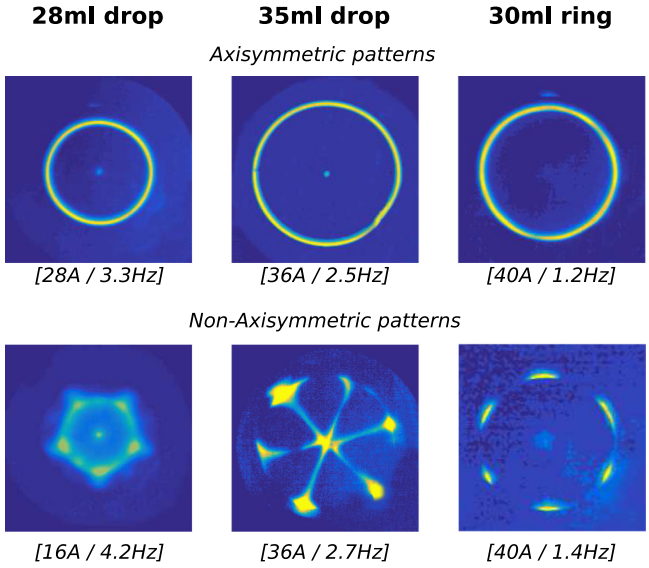

FIG. 2. Examples of patterns recovered. Each column corresponds to a fluid layer geometry (from left to right, small drop, large drop, and ring). The top (respectively, bottom) row corresponds to axisymmetric (respectively, non-axisymmetric) patterns. (A pseudo-color map has been used to improve the visibility of the patterns, but it has no direct physical interpretation.)

between the generation of the magnetic field by the retro-action of the first term on the r.h.s of Eq. (2) over the diffusive term on the Induction equation. In this problem, the magnetic Reynolds number is very small, and so the induced magnetic field is dominated by the oscillation of the external magnetic field and not by the retro action of the velocity on the magnetic field. So, for the experimental parameter ranges accessible in this experiment, the only relevant parameter is the interaction parameter N. The values attained range from $N = 0.001$ to $N = 0.2$.

B. Patterns

All the studied geometries are axisymmetric. For that reason, when the magnetic field is non-zero, the induced currents emerge in the azimuthal direction leading to radial Lorentz forces. The Lorentz forces expand and contract the droplet radius producing a beating with a frequency twice the excitation frequency $f_L = 2f_0$ that can trigger the creation of different patterns.

Looking from above to the drop surface, the liquid metal remains as a mirror when the system is at rest and there are no magnetic forces. When the external magnetic field is on, for the most part of the frequencies explored of the parameter space, an axisymmetric pattern appears, but for some frequencies non-axisymmetric structures are created. These patterns may present different azimuthal (m) wavenumbers and in some cases can display a radial wavelength (Fig. 2).

Although it is not possible to study the velocities and displacements inside the liquid metal because of the proposed optical system, we can recover the dynamical behavior of the surface modulations through the periodic acquisition of snapshots of the droplet beating. Each image has information about the surface wave amplitudes in the horizontal plane $A_i(x, y)$. So, the whole set of snapshots A_i will inform us about the dynamics in the temporal dimension $A(x, y, t)$. From these data, we can extract the frequency spectrum and we study the main harmonics that govern the dynamics of the different observed patterns.

IV. RESULTS AND DISCUSSION

A. Instabilities triggered in a fluid drop at different volumes

The first vessel geometry studied is a plate with a small depression in the central region. Due to this geometry and the surface tension effects, the fluid drop adopts the form of a thick circular layer that remains centered in the cylindrical cavity. In order to test the effect of different disc sizes, we compare the results obtained using two different InGaSn volumes, drops of 35 ml ($r_d = 40$ mm and $h_d = 22$ mm) and 28 ml ($r_d = 35$ mm and $h_d = 11$ mm).

In both cases, the first patterns observed when the magnetic field is applied are axisymmetric for almost all the parameter space. Non-axisymmetric patterns emerge in restricted frequency windows of the parameter space with different azimuthal wave numbers. For large drops of fluid, these non-axisymmetric patterns combine azimuthal and radial wavenumbers, while for small drops no radial wavelengths are observed (Fig. 3).

In a recently published work, we extensively studied the parameter space of the 28 ml drop. We noted in this work that the presence of non-axisymmetric patterns depends on two clearly differentiated pattern formation mechanisms associated with odd and even modes of the forcing frequency f_0: surface waves that evolve according to a Mathieu-Hill equation at sub-harmonic frequencies of the Lorentz frequency (please note that this frequency is twice the magnetic field frequency $f_L = 2f_0$) for odd modes and surface waves with the same frequency of the Lorentz mechanism for even modes.[11] The even-mode mechanism corresponds to the breaking of the axisymmetry for the beating of the drop, which excites surface waves with the same frequency of the forcing mechanism. The odd-mode mechanism was predicted by Refs. 10 and 19 and is a consequence of the oscillatory nature of the bulk Lorentz force.

In many experimental systems, the instabilities are characterized through the evolution of the amplitude of the fundamental mode, even if the oscillation is not harmonic. In this work, the waves are not sinusoidal but also their shape changes depending on the distance to the threshold (see Fig. 6). So, in order to characterize the instability, we have used the cumulative energy as bifurcation parameter. This cumulative energy is computed for sets of modes that share the same evolution with the intensity of the magnetic field $E_{odd} = \sum_{i=1}^{n_o} |A^2_{(2i+1)}|; E_{even} = \sum_{j=1}^{n_e} |A^2_{(2j)}|$. A total cumulative energy of the non-axisymmetric pattern can be computed as $E = E_{odd} + E_{even} = \sum_{i=1}^{n} |A_i^2|$. The threshold position is determined when the accumulated energy for the non-axisymmetric patterns overcomes the value of the noise level of the acquisition system. Using this approach, we have obtained the thresholds plotted in Fig. 4 (blue and orange solid lines). These lines split the parameter space into two parts: the axisymmetric and non-axisymmetric regions. Unfortunately,

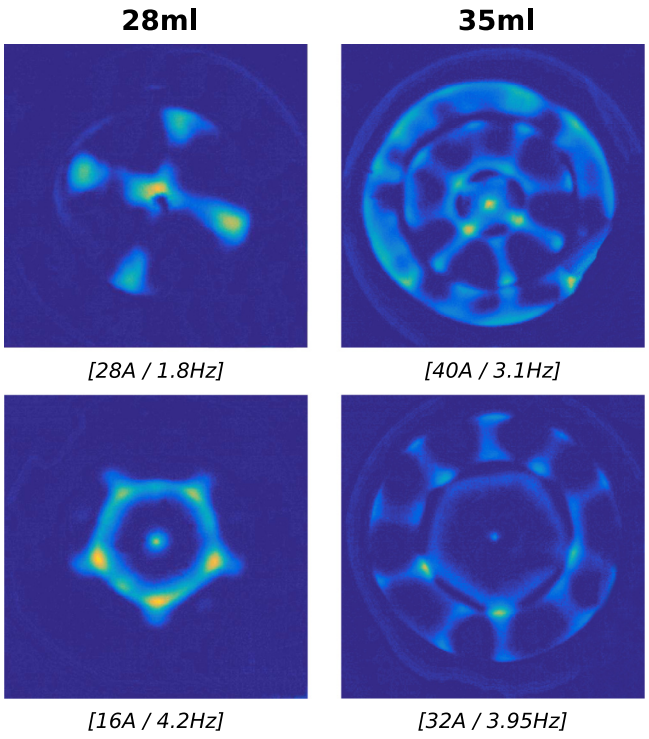

FIG. 3. Two examples of non-axisymmetric patterns ($m = 4$ and $m = 5$) for different volumes of InGaSn drop. For small volumes (left column), the patterns present pure azimuthal wavenumbers. For large volumes (right column), we observe that non-axisymmetric patterns with similar azimuthal wavenumber present a radial wavenumber. (A pseudo-color map has been used to improve the visibility of the patterns, but it has no direct physical interpretation.)

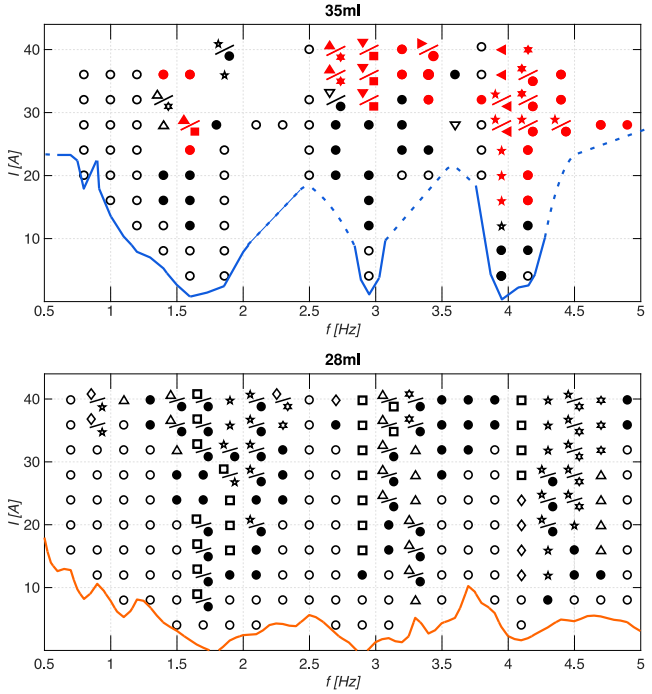

FIG. 4. Threshold boundary and observed patterns for the 35 ml and 28 ml InGaSn drops. The instability threshold, represented with a blue (large drop) and orange (small drop) line, separates regions where the pattern is axisymmetric (empty region) and non-axisymmetric (each observed pattern is marked with a different symbol). The azimuthal wavenumber is encoded as follows: ◇, $m = 2$; △, $m = 3$; □, $m = 4$; ⋆, $m = 5$; ✡, $m = 6$; ▽, $m = 8$; ▷, $m = 9$; ◁, $m = 10$. When various patterns coexist for the same parameter space point, the corresponding symbols appear separated by a slash. Circular symbols represent other non-axisymmetric patterns whose wavenumber cannot be univocally determined. Void symbols represent stable patterns, full symbols time-dependent patterns. The red symbols present on the top panel correspond to patterns that present a defined radial wavelength.

we do not have enough data from the large drop to compute the complete threshold boundary. A dashed line is used when the available data are inconclusive.

The local minima of the threshold boundaries for both cases, the 28 ml and 35 ml volumes, present slight differences. While the small volume has local minima for $f_0 = 1.8, 2.9, 4.1$, and 5.4 Hz, these minima are displaced for the big volume to $f_0 = 1.6, 2.9$, and 3.95 Hz (Fig. 4). These values agree with the interpretation provided in a previous work.[11] The excited patterns correspond to a discrete set of azimuthal wavenumbers that, due to the dispersion relation of the surface waves, fix the corresponding frequency (Fig. 5).

However, it is possible to compute the evolution of the main harmonics that govern the dynamics of the patterns in both cases. We obtain a clear power law for the bifurcation process for all the considered frequencies (Fig. 6). In all the cases, we obtain a very similar slope, with a value of 2.97 ± 0.59. This value is very different to a classical bifurcation (as, for example, a supercritical bifurcation, i.e., a dependency with a power 1/2 of the bifurcation parameter ϵ), but this difference can come from the optical setup.

Finally, we can study the amplitude of the patterns for the smallest magnetic field used in our experiment. At low intensity, the amplitude associated to the mode $2f_0$ (that corresponds to the Lorentz frequency) increases when the forcing frequency approaches some specific values. These values correspond to resonances of the minima cited above, where the corresponding wavelengths satisfy the equation $n\lambda = 2\pi R$. When the magnetic field intensity is increased, these peaks broaden, and a rich dynamics can be observed in the experiment (Fig. 7).

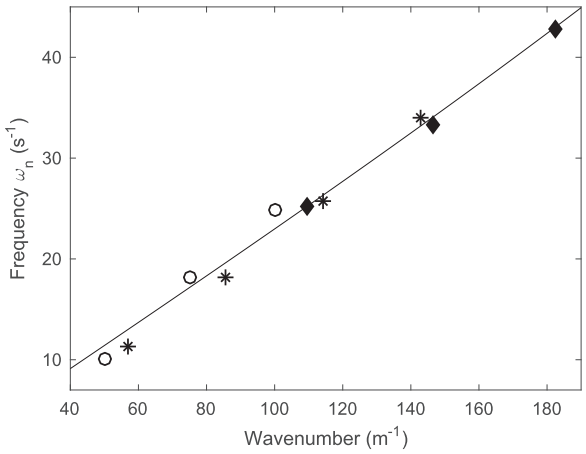

FIG. 5. Dispersion relation obtained for the excited waves at the minima observed of the threshold boundaries: the solid line represents the analytical solution; ∗ corresponds to the 28 ml drop of InGaSn even modes; ♦ corresponds to the odd modes of the same volume; ○ corresponds to the even modes of the 35 ml drop.

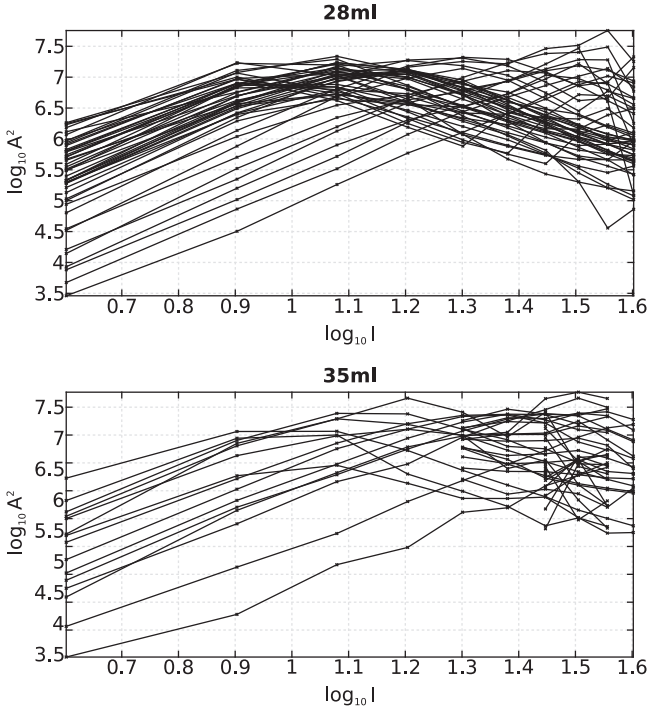

FIG. 6. Power laws observed for both InGaSn volumes 28 ml case (top panel) and 35 ml case (bottom panel): the power laws follow the same trend. Each line represents the amplitude evolution of the main harmonic at different studied frequencies.

B. Instabilities triggered in a ring geometry

In this section, we extend the study to a different geometry, the toroidal volume formed in a ring cavity. All the results presented here correspond to a 30 ml InGaSn ring.

The mechanism that triggers the instabilities follows the same physical principle: azimuthal currents created in the fluid lead to radial Lorentz forces that produce the beating of the InGaSn ring. The boundary conditions are slightly different and could alter the previously observed behavior. Apart from the fact that now the drop is toroidal, the confinement due to the bottom plate is slightly more restrictive. On the disc-shaped drops, the bottom plate was flat, but here the walls are tilted, and the beating of the drop will fight against gravity.

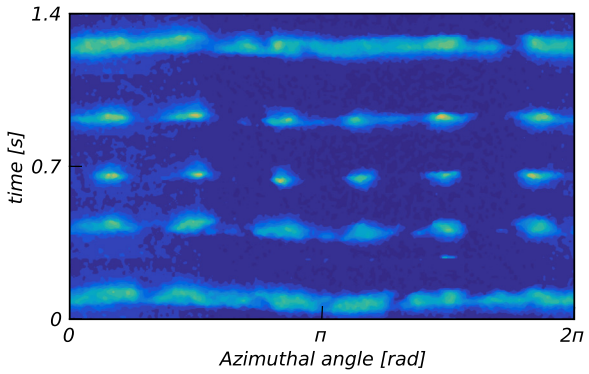

FIG. 8. Spatiotemporal evolution of a ring pattern. Each horizontal line corresponds to a snapshot of a circumference centered with the cavity axis. We can observe how a non-axisymmetric pattern with $m = 6$ is periodically excited in the experiment. (A pseudocolor map has been used to improve the visibility of the patterns but it has no direct physical interpretation.)

Although we have not been able to recover the parameter-space or to compute the instabilities threshold, we have observed different azimuthal standing waves (Fig. 2, right column). The patterns' evolution is defined recording the evolution of a circumference aligned with the cavity center. As in previous geometries, for almost all the frequencies of the parameter-space, the axisymmetric pattern is visible. But again, even in the toroid volume, there are symmetry breaking patterns with different modes that emerge for specific points of the parameter space (Fig. 8). Unfortunately, due to the limitations of the optical setup, it is very difficult to characterize the parameter space as we have done for the large drops. So, we must restrict ourselves in this geometry to a simple characterization of the existence of symmetry breaking patterns.

C. Numerical results

Both proposed mechanisms rely on an external driving force that triggers the instabilities. A classical model for the description of the envelope of a wave forced with a 1:1 driving mechanism will obey the following equation:

$$\partial_t A = \epsilon A - |A|^2 A + \partial_{xx} A + \xi,$$

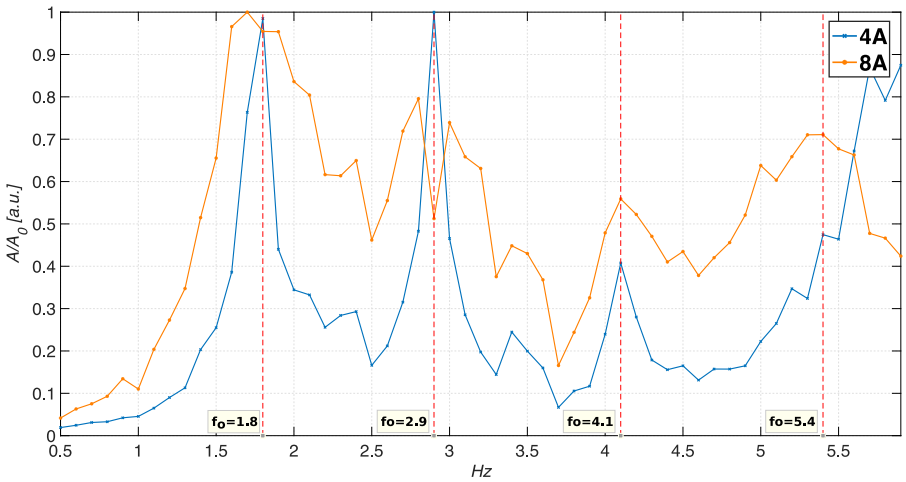

FIG. 7. Amplitude of the dominant mode in the 28 ml drop for two different forcing magnetic fields. The dashed lines represent the places where the threshold has its smaller values.

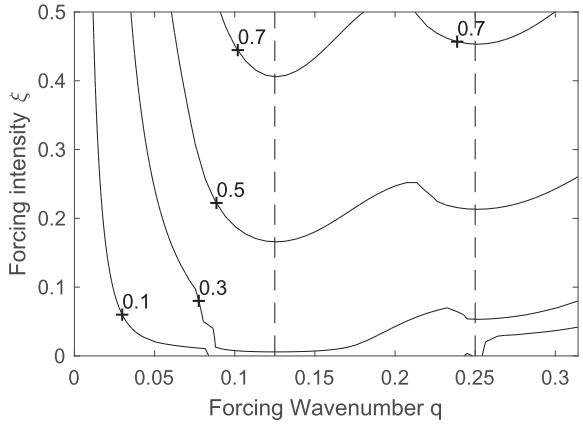

FIG. 9. Parameter space for the model: Final amplitudes obtained for each parameter set. The dashed lines represent the wavenumbers available for the numerical box.

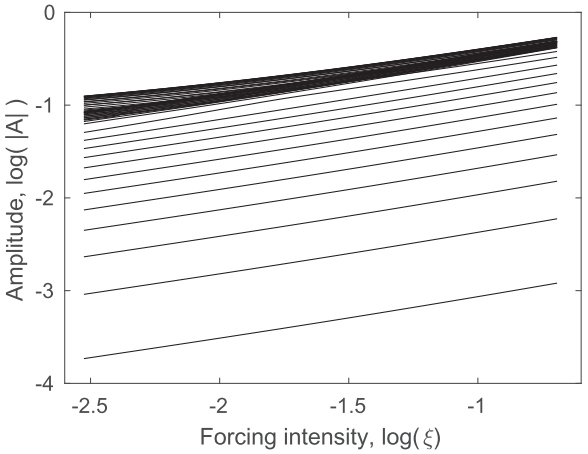

FIG. 10. Evolution of the final amplitude *vs*. the forcing intensity.

where ξ is the forcing parameter. In our problem, one of these mechanisms obeys a Mathieu-Hill equation, but the generic form of this equation as it was presented in Refs. 10 and 11 has no spatial evolution. On the other hand, in our experiment, the small aspect ratio imposes a discretization of the available wavenumbers and becomes a key feature of the dynamics, so any potential model to reproduce our results must reflect this behavior. Having in mind these experimental results, we propose a model for the 1:1 mechanism that was inspired on a previous experiment with spatial forcing:[18]

$$\partial_t A = \{\epsilon + \xi \exp(i\,q\,x - \Phi)\}\,A - |A|^2 A + \partial_{xx} A,$$

where again ξ is the forcing amplitude, q is the wavenumber produced by the forcing oscillation, and Φ is the phase of the complex amplitude A. We have tested the response of this model to different wavenumbers and different forcing values. All the results were computed using $N = 512$ points in a box of size of $L = 50$. Each simulation run lasted for $T = 500$ time units.

In Fig. 9, we represent the final amplitude recovered for each point of the parameter space. From these data, we observe that the final solution reaches a larger value in the neighborhood of the resonant wavenumbers, as it happens on the experiment. But probably the most important result is that we cannot observe any real threshold for any wavenumber. There is always a residual amplitude even if we are far from the resonances.

In Fig. 10, we represent the dependence of the amplitude of the final solution vs. the forcing intensity. Here, we recover the expected behavior of a power law, similar to the experimental result, but here the exponent is $1/2$ as expected.

D. MHD effects in the semicircular ducts of the inner ear

It was noted in some recently published experimental works that some patients refer adverse symptoms (i.e., vertigoes and dizziness) when they are subjected to MRI high magnetic fields.[16,17] These works explain their result as the interaction of the external magnetic fields with ionic currents present on the inner ear, the location where the sense of balance is placed.

These authors neglect a pure MHD origin because they assume that these forces should be very weak. However, our results reveal that even for interaction parameter values N comparable to the ones of the inner ear, there are instabilities that can be triggered. If we assume as a typical value applied in an MRI device as 3 T and a minimum frequency of 4 Hz, the estimated maximum semicircular duct N value is 0.0011. In our experiment, these values are able to trigger symmetry breaking patterns, so pure MHD effects cannot be neglected as the origin of these adverse symptoms.

Finally, the results presented in this work reveal that the instability does not depend on the shape of the conducting fluid drop. Even in the toroidal case, the one that is closer to the inner ear configuration (where the conducting fluid is an electrolyte), we can observe patterns created for interaction parameter values similar to those attained in the cochlea in a MRI device.

V. CONCLUSION

We have presented results of an experiment where a liquid metal layer with different geometries is forced by a time-dependent magnetic field. All the geometries are axisymmetric, so the physical mechanisms that trigger the instabilities are produced by radial Lorentz forces that alternatively push and contract the fluid drop with a frequency twice the excitation frequency of the system.

For the disc-shaped drop, we have observed an axisymmetric pattern present for almost all the frequencies of the parameter-space. For some restricted regions of this space, there are patterns that break the azimuthal symmetry. When the volume of this drop is large enough, the beating of the drop creates patterns that also create a radial wavelength. The threshold of the instability that creates these patterns has different minima, whose position slightly depends on the considered fluid volume. When we move away from threshold, a clear power law dependency with the forcing intensity is recovered. For the torus-shaped drop, a similar behavior is obtained. Non-axisymmetric patterns have been recovered for specific values of the control parameters, while axisymmetric patterns are present elsewhere.

Our results call into question the usual approach that disregards MHD forces when the interaction parameter is smaller than $N = 0.01$. In our case, we find patterns and rich dynamics even for values one order of magnitude below that limit. A problem where this could be of particular interest is the forces that may appear in the inner ear of a person in an MRI device. Although the forces present in this case are very small, we have observed that instabilities can be triggered at low interaction parameter values. So, MHD forces cannot be dismissed on those systems.

ACKNOWLEDGMENTS

The authors acknowledge the support of the Spanish Government through Grant Nos. FIS2014-54101-P and FIS2017-83401-P. One of the authors (I.C.D.) acknowledges Asociación de Amigos de la Universidad de Navarra for a research grant.

[1]M. Faraday, "On a peculiar class of Acoustical figures; and on certain forms assumed by groups of particles upon vibrating elastic surfaces," Philos. Trans. R. Soc. Lond. **121**, 299–340 (1831).
[2]T. B. Benjamin and F. Ursell, "The stability of the plane free surface of a liquid in vertical periodic motion," Proc. R. Soc. Lond. A **225**, 505–515 (1954).
[3]J. Rajchenbach, D. Clamond, and A. Leroux, "Observation of star-shaped surface gravity waves," Phys. Rev. Lett. **110**, 094502 (2013).
[4]J. M. Galpin, Y. Fautrelle, and A. D. Sneyd, "Parametric resonance in low-frequency magnetic stirring," J. Fluid Mech. **239**, 409–427 (1992).
[5]J. Burguete and M. A. Miranda, "Instabilities of conducting fluid layers in cylindrical cells under the external forcing of weak magnetic fields," Magnetohydrodynamics **48**, 69–75 (2012).
[6]E. Ramírez-álvarez, J. L. Ocampo-Espindola, F. Montoya, F. Yousif, F. Vázquez, and M. Rivera, "Extensive study of shape and surface structure formation in the Mercury beating beart system," J. Phys. Chem. A **118**, 10673–10678 (2014).
[7]I. Cortés-Domínguez, J. Burguete, and H. L. Mancini, "Experimental dynamics in magnetic field-driven flows compared to thermoconvective convection," Philos. Trans. R. Soc. Lond. A **373**, 2056 (2015).
[8]C. L. Shen, W. J. Xie, and B. Wei, "Parametrically excited sectorial oscillation of liquid drops floating in ultrasound," Phys. Rev. E **81**, 046305 (2010).
[9]J. M. Galpin and Y. Fautrelle, "Liquid-metal flows induced by low-frequency alternating magnetic fields," J. Fluid Mech. **239**, 383–408 (1992).
[10]Y. Fautrelle and A. D. Sneyd, "Surface waves created by low-frequency magnetic fields," Eur. J. Mech. - B/Fluids **24**, 91–112 (2005).
[11]I. Cortés-Domínguez and J. Burguete, "Instabilities of conducting fluid layers in weak time-dependent magnetic fields," Phys. Rev. E **96**, 013103 (2017).
[12]N. B. Morley, J. Burris, L. C. Cadwallader, and M. D. Nornberg, "GaInSn usage in the research laboratory," Rev. Sci. Instrum. **79**, 056107 (2008).
[13]Y. Plevachuk, V. Sklyarchuk, S. Eckert, G. Gerbeth, and R. Novakovic, "Thermophysical properties of the liquid GaInSn eutectic alloy," J. Chem. Eng. data **59**, 757–763 (2014).
[14]W. Merzkirch, *Flow Visualization* (Academic Press Inc., 1987).
[15]R. J. Moreau, *Magnetohydrodynamics* (Springer, 1990).
[16]D. C. Roberts, V. Marcelli, J. S. Gillen, J. P. Carey, C. C. Della Santina, and D. S. Zee, "MRI magnetic field stimulates rotational sensors of the brain," Curr. Biol. **21**, 1635–1640 (2011).
[17]B. K. Ward, D. C. Roberts, C. C. Della-Santina, and P. Carey, "Vestibular stimulation by magnetic fields," Ann. N. Y. Acad. Sci. **1343**, 69–79 (2015).
[18]M. Henriot, J. Burguete, and R. Ribotta, "Entrainment of a spatially extended nonlinear structure under selective forcing," Phys. Rev. Lett. **91**, 104501 (2003).
[19]K. Spragg, A. Sneyd, and Y. Fautrelle, "Mathematical analysis of the oscillations of a liquid metal drop submitted to low frequency fields," Magnetohydrodynamics **45**, 543–548 (2009).